Development of a Bridge Inspection Robot Capable of Traveling on Splicing Parts

Yogo Takada, Satoshi Ito and Naoto Imajo

inventions

MDPI

Article

Development of a Bridge Inspection Robot Capable of Traveling on Splicing Parts

Yogo Takada *, Satoshi Ito and Naoto Imajo

Department of Mechanical and Physical Engineering, Osaka City University, Osaka 558-8585, Japan; ito_satoshi_01@yahoo.co.jp (S.I.); efil.ym.yojne0723@gmail.com (N.I.)

* Correspondence: takada@eng.osaka-cu.ac.jp; Tel.: +81-6-6605-2970; Fax: +81-6-6605-2769

Received: 21 July 2017; Accepted: 23 August 2017; Published: 26 August 2017

Abstract: Several infrastructures, such as bridges and tunnels, require periodic inspection and repair to prevent collapse. There is a strong demand for practical bridge inspection robots to reduce the cost and time associated with the inspection of bridges by an inspector. Bridge inspection robots are expected to pass through obstacles such as bolted splice part and right-angled routes. The aim of this study involved developing a bridge inspection robot that can travel on a right-angle path as well as splicing parts. A two-wheel-drive robot was developed and equipped with two rimless wheels as driving wheels. A neodymium magnet was provided at the tip of each spoke. Non-driving wheels were attached at the rear as a rotatable caster. The robot can turn on the spot to avoid the bolt on the splicing part. Experiments were conducted to check the performance of the robot. The results confirmed that the robot passed through the internal right-angle paths in a laboratory and in an actual environment that corresponds to a box girder of a bridge. It is extremely difficult to manually control a robot on the splicing part. Therefore, a camera and an LED (light emitting diode) were attached to autonomously control the robot. The results indicate that the newly developed robot could run through the splicing part without hitting the nuts.

Keywords: moving robot; bridge inspection; steel bridge; magnet; bolt; splicing part; two-wheel-driven robot; right-angle path; rimless wheel

1. Introduction

Social infrastructures, such as bridges and tunnels, that have been constructed in various places are vital to the daily lives of people. However, there is a decrease in their functionality over time. Bridges are designed to withstand the load of running vehicles for over 50 years after their construction. However, an increase in the number of bridges over 50 years old is expected in the near future. The measures for old bridges constitute a significant challenge. It is not easy to renew the large infrastructures given the time and financial resources required to do so. Thus, performing periodic inspections, determining damaged areas early, and repairing any such areas to maintain the infrastructures to the maximum possible extent constitute a realistic option. Thus, lifecycle management to maintain bridge structures is important [1].

For example, the number of aging infrastructures is increasing in Japan. Japanese bridges and tunnels were constructed during a period of high economic growth. Currently, a first inspection of bridges is required within two years of use, and a periodic bridge inspection is then performed once every five years from the second time onward [2]. The inspectors must investigate damage conditions including corrosion, cracks, bolt loosening, falling bolts, and breakages for all members in all spans. After this, it is necessary to perform four levels of judgment with respect to the soundness of each member. Periodic inspections are based on visual observation by inspectors that use scaffolding or a special-purpose vehicle. Therefore, each local government is burdened with the tremendous costs associated with performing such inspections.

Recently, various robots have been developed for bridge inspection to reduce the burden of periodic inspection. Since 2015, a multi-rotor helicopter has become an attractive and suitable option for bridge inspections, and has been examined by several studies [3–5]. In the case of steel bridges, as magnet adhere to the structure, a robot equipped with magnets is more suitable for inspecting the lower side of the bridge in detail. However, difficulties exist with respect to the detailed inspection of several members located under the steel bridge structure. Therefore, there is a demand for a robot that moves to a target location and delivers photographs of each part of the bridge. Since the inspection of a steel bridge is mainly based on the visual inspection, it is required that the robot does reduce the ability to move in all directions, even if the camera is fixed on a mount.

Many robots can move along the flat parts of a ceiling surface or can climb up and down a wall to avoid falling due to gravity [6–9]. For example, a flexure-based mobile sensing node (FMSN) developed by Zhu et al. is able to climb a wall and then continue to run on the surface of a floor [8]. However, it is difficult to change the travel course in the left and right directions in the FMSN because the magnets used in this robot include a large ground contact area.

Robots named "BIREM" were also developed to move in complex environments under steel bridges to inspect cracks and corrosion areas. BIREM moves while adsorbing to the steel wall using a rimless wheel with attached magnets [10,11]. Additionally, BIREM has a high success rate while traveling between a ceiling and a vertical wall. Furthermore, it is possible to change the course in the left and right directions with the steering mechanism on the front and rear wheels attached to second generation BIREM (BIREM 2nd) because of the small ground contact area of the magnets.

Steel bridges are constructed by joining several steel plates with bolts. However, the splicing parts with many bolts hinder the path of robots. It is not possible for BIREM 2nd to run on this route. Moreover, to the best of the authors' knowledge, extant studies have not examined whether it is possible for a robot to run on routes that include splicing parts. Therefore, in this study, the latest generation BIREM (BIREM 3rd) is developed with the aim to run it on a right-angle course as well as to run it on the splicing parts of a bridge.

2. Required Bridge Inspection Robots

2.1. Performance Requirements for Robots

Currently, bridge inspection is conducted by inspectors. A few items are required so that a robot can perform this work. In this study, points (1) to (4), which are discussed below, are considered, although the specific aim of the development of the robot corresponds to (1).

(1) Ensuring a moving ability that can overcome any obstacles in the inspection environment.

(2) Ensuring a climbing ability even if the robot is equipped with a sensor to detect cracks and corrosion.

(3) Ensuring an ability to inspect for a long time.

(4) Ensuring an ability to withstand disturbances such as the vibration of a bridge by automobiles or a strong wind at a high altitude.

2.2. Splicing Parts in a Box Girder

One of the main purposes of the study is to develop a robot that runs through the splicing parts of a bridge. Figure 1 shows the splicing parts with several bolts on the ceiling inside a box girder of a bridge. Bridge inspection robots are required to run along a path, including splicing parts, to inspect a bridge. The bolts of the splicing parts completely block the traveling path of the robot. Therefore, it is not possible for a robot to run through the traveling path in the absence of measures for the splicing parts. For example, it is not possible for previously developed robots [8,9] or old-type BIREM [10] introduced in Section 1 to run through the splicing parts because there are no measures set in place to overcome this obstacle.

Figure 1. The bolted splicing part in the box girder of a bridge.

3. Structure of the BIREM 3rd Robot

3.1. How to Run through the Splicing Part

Figure 2 shows the physical relationship between the wheel track of a new prototype robot named BIREM 3rd and the bolts on the splicing parts. The size of bolts used in steel bridges in Japan mostly corresponds to M22 or M24. The interval of the bolts on the splicing parts was examined [12]. In the specifications for highway bridges, the minimum bolt intervals for M22 and M24 correspond to 75 and 85 mm, respectively. However, if it is unavoidable with respect to the design of the bridge, the bolt intervals for M22 and M24 can correspond to 66 and 72 mm, respectively. While manufacturing a robot, it is easier to design and manufacture a wide wheel track. However, the wheel track is fixed at 74 mm such that the robot can run through the splicing part in which the bolt interval corresponds to 66 mm. Additionally, as BIREM 3rd runs through the splicing part, each bolt relatively passes through the space under the lower part of the robot's main body in a successive manner.

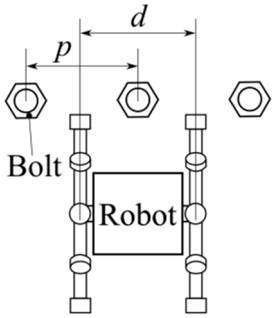

Figure 2. Bolt pitch of splice part. The length d is the wheel track of the robot and the length p is the interval of the bolts.

Furthermore, it is also necessary to consider the height direction of the bolts and nuts to avoid collision with bolts or nuts. The splicing part connects the plates with bolts, nuts, and washers. Therefore, especially on the nut side, it is necessary to prevent the height of the nut as well as the threaded portion of the bolt from the nut center from hitting the main body of the robot. For this reason, the vehicle height is designed such that it is sufficiently high to pass over the nuts, at 70 mm.

3.2. Configuration of BIREM 3rd

Figure 3 shows the appearance of the bridge inspection robot BIREM 3rd that is manufactured based on the concept discussed in Section 3.1, and Figure 4 shows the configuration. The main body

of the robot consists of CFRP (Carbon Fiber-Reinforced Plastic) and acrylic material to ensure that it is light. Table 1 shows the specifications of BIREM 3rd. The total length corresponds to 245 mm, the width corresponds to 80 mm, the total height corresponds to 133 mm, and the weight corresponds to 411 gf. The wheel track is set as small as possible at 74 mm, based on the M22 or M24 bolts on the splicing parts. Subsequently, the vehicle height is set high such that the main body does not hit a bolt or a nut. A robot with a small wheel track and a high vehicle height possesses poor running ability and poor turning ability when compared with a robot with a large wheel track and a low vehicle height. However, running through the splicing parts constitutes a top priority to practically use the bridge inspection robot. The main controller, FPGA (Field-programmable gate array), Xilinx XC6SLX45 CSG324, and the receiver (Futaba R2106GF) are installed, thus making it possible to remotely control the robot with an external transmitter, namely, Futaba T6J. The power source corresponds to a lithium polymer battery with two cells rated at 7.4 V, 800 mAh. Additionally, a camera and an LED (Light emitting diode) are attached for autonomous driving. The details are described in Section 4.

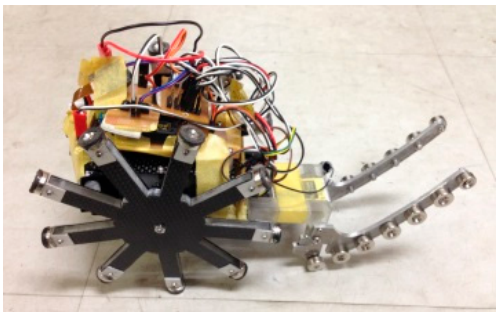

Figure 3. Bridge inspection robot (BIREM 3rd).

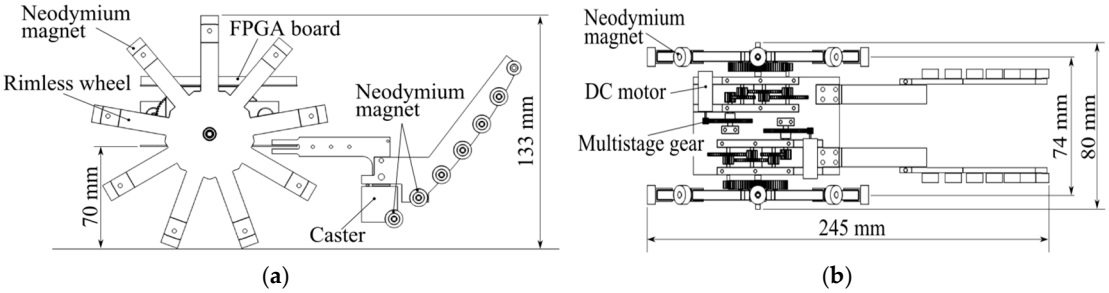

Figure 4. Mechanism of BIREM 3rd. (**a**) Side view; (**b**) top view.

Table 1. Specifications of BIREM 3rd. FPGA, field-programmable gate array.

Property	Specifications
Length	245 mm
Width	80 mm
Total height	133 mm
Vehicle height	70 mm
Wheel track	74 mm
Weight	411 gf
Controller	FPGA (Spartan-6)

This robot runs using the large wheels at the left and right connected to the direct current motors via gears. A neodymium magnet is attached at the tip of each spoke. A rubber coating exists on the magnet surface at which a magnet is in contact with the floor, wall, or ceiling. This robot can climb the wall because the permanent magnet is chosen so that the frictional force between the rubber coated

on the magnet and the steel wall is larger than the robot weight. Additionally, rimless wheels are manufactured by molding an ultraviolet curable resin, and the surface is reinforced with CFRP (Carbon fiber reinforced plastic) plates with a thickness of 0.2 mm.

On the rear part of the robot, seven non-driving wheels that correpsond to cylindrical neodymium magnets are attached to the left and right. Specifically, the front most wheel rotates freely in the left and right directions. The 14 non-driving wheels are described in Section 3.3.

3.3. Enhancing Running Ability and Turning Ability

The wheel track is small and the vehicle height is high; thus, ingenuity is necessary to enhance running ability and turning ability. The running ability is defined as the ability to run the robot without it dropping from a ceiling or a wall.

It is difficult for a robot to avoid running on a bolt on the splicing parts unless the turning ability is high. In a manner similar to a passenger car, a four-wheeled robot cannot turn on the spot, and thus, it does not possess sharp turning ability. Therefore, BIREM 3rd is developed such that it can travel with two wheels and can turn on the spot. However, with respect to the left and right two-wheel robots, rear wheels are required to support the main body to prevent rotation due to the reaction torque generated when the main wheels are rotated. Figure 5 shows the postures when a two-wheel robot, such as BIREM 3rd, moves up and down the wall. When the robot ascends or descends on the wall surface, the robot experiences a moment of force due to the gravity centered on the rotating point as shown in Figure 5. In the case when the robot ascends the wall, the moment of force due to gravity is supported by the non-driving wheels at the rear as shown in Figure 5a, and thus, the robot can move upward. However, in the case when the robot descends the wall, the moment of force due to gravity cannot be supported if the rear wheels are not in contact with the wall surface, and thus, the robot falls down from the wall as shown in Figure 5b. Specifically, the structure of the robot is designed with a high vehicle height such that it can run through the bolts on the splicing parts, and thus, the moment of force due to gravity is significantly high. Therefore, a very strong permanent magnet is adopted for the non-driving wheels to prevent falling. Additionally, the adsorption force makes the turning movement of the robot difficult, and thus, a caster structure is adopted, which rotates and changes the direction of the non-driving wheel at the rear.

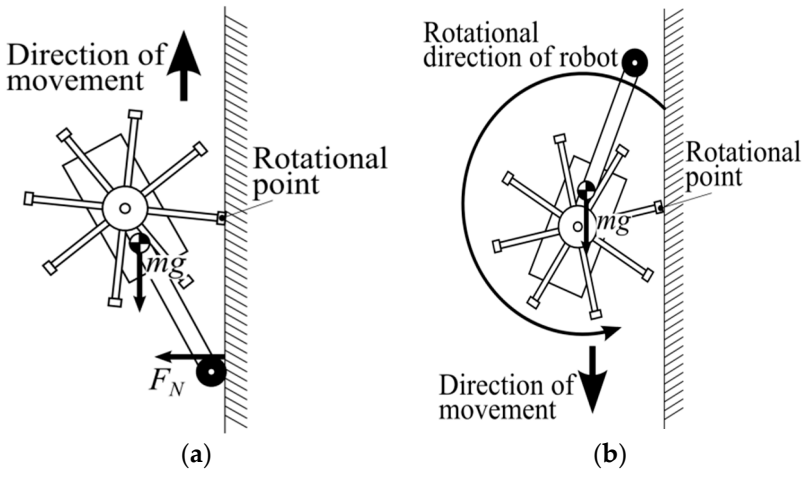

Figure 5. Attitude of the two-wheel-drive robot on the vertical wall. (**a**) Robot climbing wall; (**b**) robot moving down.

Additionally, bridge inspection robots are required to run through the splicing parts as well as on a right-angle path. If a rear wheel is attached to the main body, then the rear wheel moves with the trajectory shown in Figure 6a around the center of the drive wheel as the rotation center.

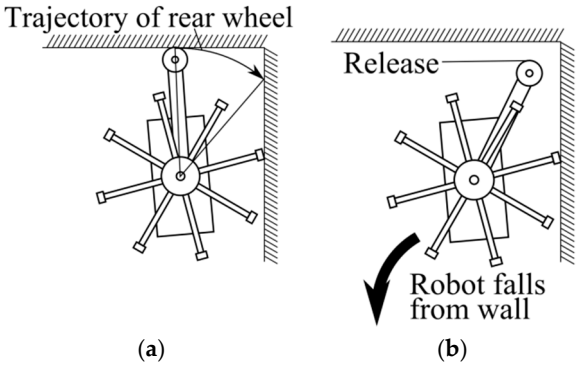

Figure 6. Robot falling from the right-angled route. (**a**) Rear wheel touching ceiling; (**b**) rear wheel releasing ceiling.

The rear magnet wheel touches the ceiling surface until it passes immediately above the center of the front wheel. However, the rear magnet wheel is subsequently released from the ceiling surface because the rear magnet wheel moves along the trajectory shown in Figure 6b. This posture is similar to the situation shown in Figure 5b, and thus, the moment of force due to gravity decreases with respect to the wall. To prevent this fall, it is necessary for the rear wheel to touch the ceiling surface or wall surface, even when the robot runs on the right-angle path.

To prevent the robot from falling when it runs on the right-angle path, an original rear wheel system with multiple cylindrical magnet wheels arranged in an arc shape is adopted, as shown in Figure 7. The front wheel corresponds to a rotating caster, and the robot has a structure that makes it easy to turn.

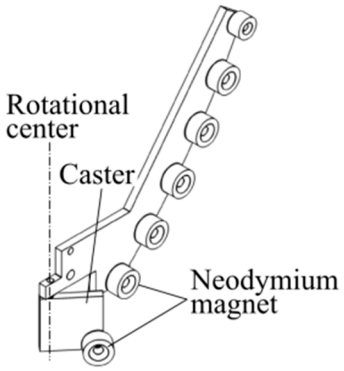

Figure 7. Magnetic rear wheels with a caster.

Figure 8 shows the manner in which the robot moves from the ceiling surface to the vertical wall surface using the rear wheel system. Figure 8a shows the state when the robot moves horizontally on the ceiling and the front wheel touches the vertical wall surface. Following this, the front rimless wheel descends the wall, and the rear wheel "B_1" comes in contact with the ceiling surface, as shown in Figure 8b. At this time, the rear wheel "B_2" does not yet touch the ceiling surface. After the rear wheel "A" leaves the ceiling, the rear wheel "B_2" soon touches the ceiling surface, as shown in Figure 8c. When the front wheel advances, the magnet wheels are repeatedly attached and detached from the rear wheel "B_2" to the rear wheel "B_5". Finally, the rear wheel "C" comes in contact with the ceiling surface, as shown in Figure 8d. Subsequently, as shown in Figure 8e, the rear wheel "B_5" is released from the ceiling surface, and the rear wheel "A" gradually approaches the vertical wall surface.

Following this, the rear wheel "A" touches the wall surface, as shown in Figure 8f. Finally, as shown in Figure 8g, the rear wheel "C" moves away from the ceiling surface, and the transition from the ceiling to the wall is completed. This original rear wheel system is used, and it is possible

for the robot BIREM 3rd to perform running through the splicing parts, sharp turning, and running through the right-angle path.

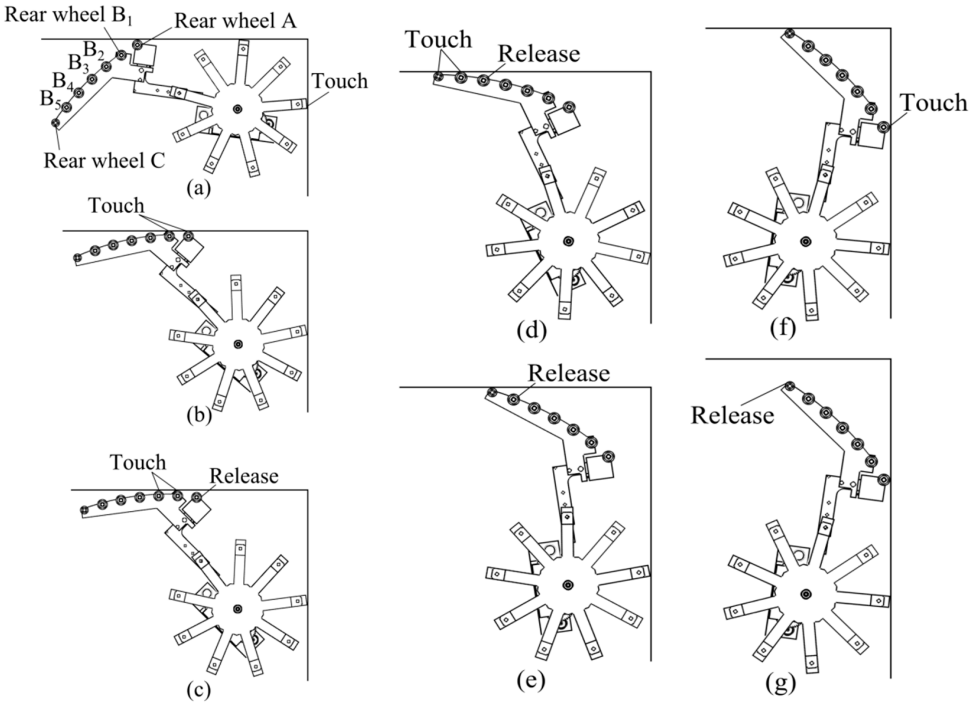

Figure 8. Robot running along the right-angled route. (**a**) Front wheel touches the vertical wall after the robot moving horizontally; (**b**) rear wheel B_1 touches the ceiling as well as the rear wheel A; (**c**) after rear wheel A released, rear wheel B_2 touches the ceiling promptly; (**d**) after rear wheel B_4 released, rear wheel C touches the ceiling promptly; (**e**) rear wheel B_5 is released from the ceiling; (**f**) while the rear wheel C is in contact with the ceiling, the rear wheel A contacts the vertical wall; (**g**) rear wheel C is released from the ceiling and the robot descends.

4. Results and Discussion for Experiments with BIREM 3rd

4.1. Experimental Results of Running on a Right-Angle Path in a Bridge Box Girder

Experiments were performed to ascertain as to whether BIREM 3rd can travel on a right-angle path under actual circumstances. The experimental environment involved using the bridge box girder, shown in Figure 9a, installed in the Earthquake museum of Hanshin Expressway Co., Ltd (Osaka, Japan). The right-angle paths where the robot travels in the experiment correspond to 1 and 2, as shown in Figure 9b.

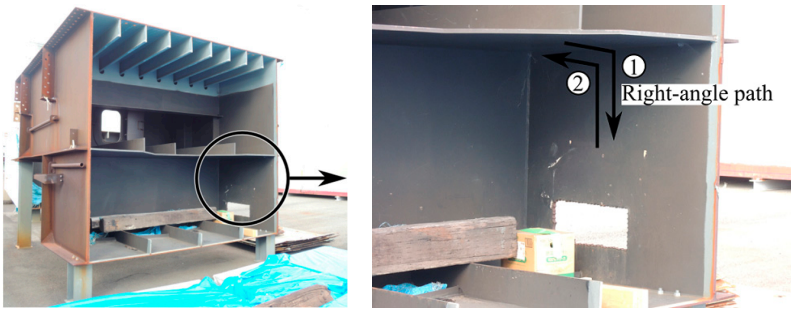

(**a**) (**b**)

Figure 9. Box girder of the bridge. (**a**) External view; (**b**) enlarged view.

Prior to performing the experiment in the field, the experiment was performed on the same routes in the laboratory, and 10 experiments were performed successfully. However, at the start time of the field experiment, the magnets on the rimless wheel slipped, and the robot was unable to even climb the wall. The box girders used for bridges are paint-treated on weather resistant steel materials to prevent corrosion. In this case, a magnetic force reduction approximately ranging from 25% to 40% exists. For example, in the laboratory steel box, the magnetic force between the bottom surface "A" of Figure 10 and steel wall corresponds to 1960 gf when the magnet diameter corresponds to 10 mm. Conversely, in the case of the box girder in the actual environment, the magnetic force only corresponds to 1180 gf given the same conditions. Table 2 shows each magnetic force with respect to the steel wall surface. When the rubber coating is applied to the magnet and the magnet is tilted with respect to the wall surface, the minimum magnetic force decreases to approximately 900 gf. Then, the friction coefficient between the rubber and the painted general steel measured around 0.35 in our experiment. In other words, the frictional force of both the left and right wheels is approximately 630 gf, which is larger than the weight of the robot (411 gf), so the magnets on each wheel do not slip. Besides, the motors mounted on the robot would allow the robot climb the wall if the total weight of the robot body and the load such as a high-resolution camera is under 545 gf. However, when the magnetic force reduces from 1960 to 1180 gf, the frictional force of both the left and right wheels becomes 380 gf. Therefore, despite the sufficient motor torque, the robot was not able to climb the wall of the box girders.

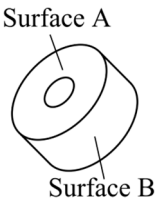

Figure 10. Neodymium magnet.

Table 2. Magnetic force to steel surface.

Size of the Magnet	**10-mm Diameter Magnet**	
Contact surface	Surface A	Surface B
Surface of the steel box in the laboratory	1960 gf	535 gf
Surface of the box girder bridge	1180 gf	405 gf
Size of the Magnet	**12-mm Diameter Magnet**	
Contact surface	Surface A	Surface B
Surface of the steel box in the laboratory	2900 gf	820 gf
Surface of the box girder bridge	1850 gf	620 gf

Thus, it is necessary to use stronger magnets. As shown in Table 2, the magnetic force for a diameter of 12 mm corresponds to 1850 gf at the bottom surface "A" and 620 gf at the side surface "B" for the wall surface of the bridge box girder. This is close to the magnetic force for a 10-mm diameter magnet for the wall surface in the laboratory. Therefore, an attempt was made to allow the robot to climb the wall by replacing the magnets with 12-mm diameter magnets. As a result, the robot was able to climb the wall in the real environment.

Figures 11 and 12 show the manner in which BIREM 3rd runs on each route. It easily travels on a right-angle path if the magnetic force is adjusted appropriately.

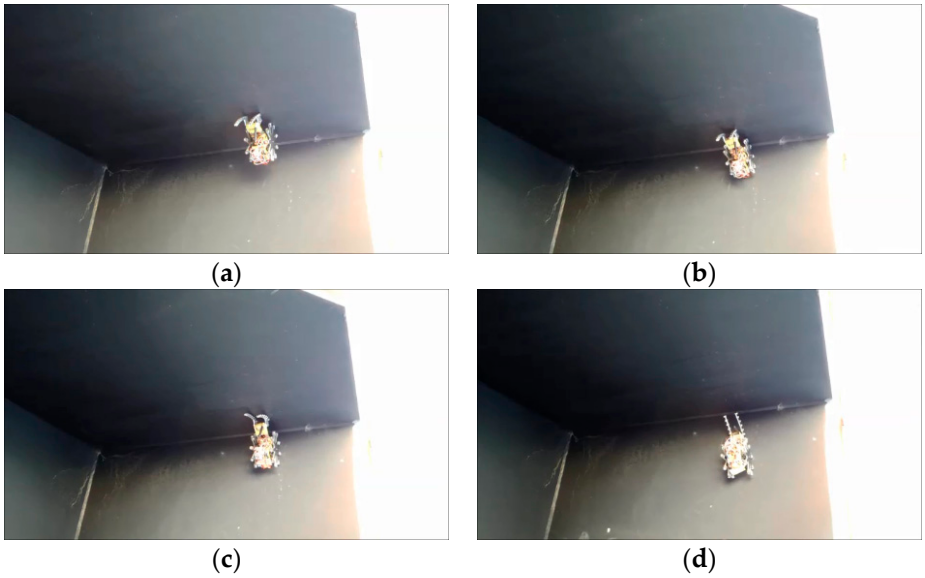

Figure 11. BIREM 3rd moving along route 1. (**a**) 0 s; (**b**) 5 s; (**c**) 10 s; (**d**) 15 s.

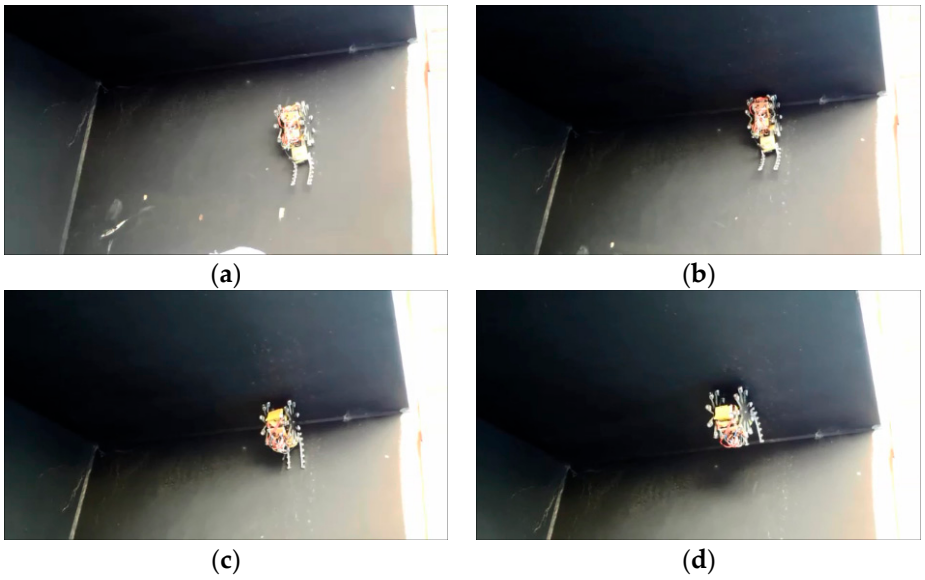

Figure 12. BIREM 3rd moving along route 2. (**a**) 0 s; (**b**) 3.3 s; (**c**) 6.7 s; (**d**) 10 s.

4.2. Experimental Results of Running on the Splicing Part

The splicing part includes several bolts and nuts. Figure 13 shows a model of a splicing part used in the experiment performed in the laboratory. Specifically, fifteen M22 nuts were placed in the same location as the splicing part in a bridge. The experiments were performed to run BIREM 3rd on the splicing part.

There is enough space for a nut to pass under the robot, and thus, it is necessary for the operator to move the robot toward the nut. It is not difficult to maneuver the robot by keeping the wheels from lifting above each nut when the operator is near the robot. However, it is extremely difficult to keep the wheels from lifting on the nuts when the operator maneuvers the robot from a distance or when the operator maneuvers the robot while watching the image from the camera installed on the robot.

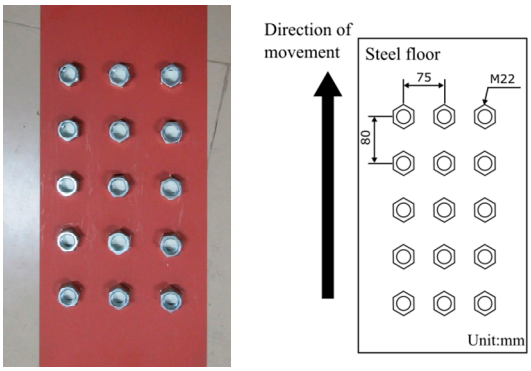

Figure 13. Model of the splicing part with 15 nuts for the experiment.

This robot includes a structure to run through the splicing parts and possesses excellent turning ability. However, it is difficult to manually adjust the traveling direction. Therefore, the robot is controlled such that it runs semi-autonomously. First, a small camera and an LED are attached to the robot. Second, a program for hardware description language was created. In this program, the FPGA sends a command to the motor based on the image acquired by the camera, and the robot itself controls the robot direction such that the robot faces a nut. The control method corresponds to a simple proportional control, and the feedback control is performed such that the illuminated nut is at the middle of the camera image.

The inside of the box girder is dark. Therefore, it is considered that the following method, using the reflection of light, is effective in estimating the position of a bolt or a nut in front of the robot.

(1) White light is illuminated with an LED in the robot's traveling direction.

(2) The bolt or nut in the illuminated range strongly reflects light, and the part is brightly displayed even in the camera image.

(3) The position of the bolt or nut is estimated based on the information in the bright part in the camera image.

The success rate of the autonomous control varies based on how the camera and LED are installed. As shown in Figure 14, the distance from the floor and the attachment angle are important. If the place to be illuminated with the LED is inappropriate, then the robot travels to the opposite direction for the nut that corresponds to a target.

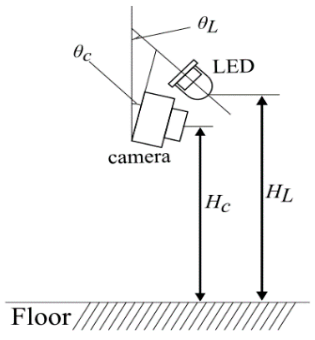

Figure 14. Position relationship between the camera and the LED attached to the robot.

Figure 15 shows the illuminated ranges of "A", "B", and "C". In the range "A" the robot turns appropriately to the left because the illuminated nut is on the left side in the camera image. However, in range "B", the lit nuts are on both sides of the camera image, and thus, it is not possible for the robot to determine the direction of the turn. Additionally, in range "C", the robot moves in the wrong direction since the lit nut is on the right side.

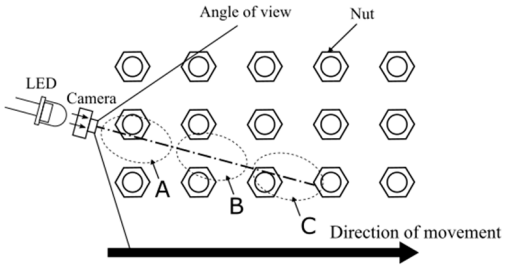

Figure 15. Position of each nut shown in the camera that changes based on the irradiation position of the LED (from A to C).

Hence, it is preferable to illuminate the nut close to the robot with the LED light. Therefore, the installation parameters in Figure 14 are defined as follows: $\theta_c = 12°$, $\theta_L = 55°$, $H_c = 85$ mm, $H_L = 91$ mm.

Running experiments were conducted with the model of the splicing parts. Gears were used to transmit torque to the driving wheels of BIREM 3rd. The positional relationship of either the left or right gear was adjusted to reduce the transmission efficiency of the torque, and thus, the robot cannot run straight. Figures 16 and 17 are images of the camera attached to the front of BIREM. This autonomous control to run without riding on a nut uses the camera and FPGA attached to the robot. However, we were not able to determine how controller performed based on the image. Therefore, the camera images have been encoded, transferred, decoded, and projected on the external TFT (thin-film transistor liquid-crystal display) to confirm the status of the autonomous control in real time. However, like in Figure 17, sometimes projecting on the TFT fails when transferring images taken in the dark. The image transfer failed on the gray rectangular parts in Figure 17. Figure 16 shows the experimental result when the robot that cannot run straight and does not possess a steering control system is used. This figure shows the camera image taken by the robot every 1 s when running on the splicing part model. After 2 s, the robot gradually turned away to the right, and the wheel ran on a nut at 4 s. Figure 17 shows the camera images every 2 s when the steering control system is used. The images indicate that the robot can travel successfully on the splicing part. In the experiment, the operator provides only the forward direction speed command from the transmitter, and the rotation direction is autonomously controlled.

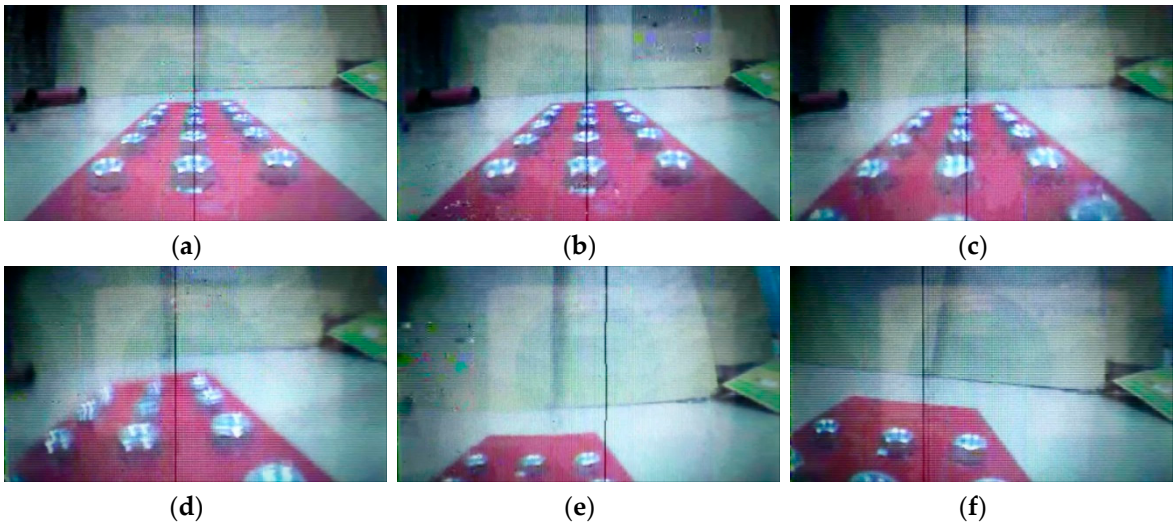

Figure 16. Images of camera attached to the front of BIREM without the control. (**a**) 0 s; (**b**) 1 s; (**c**) 2 s; (**d**) 3 s; (**e**) 4 s; (**f**) 5 s.

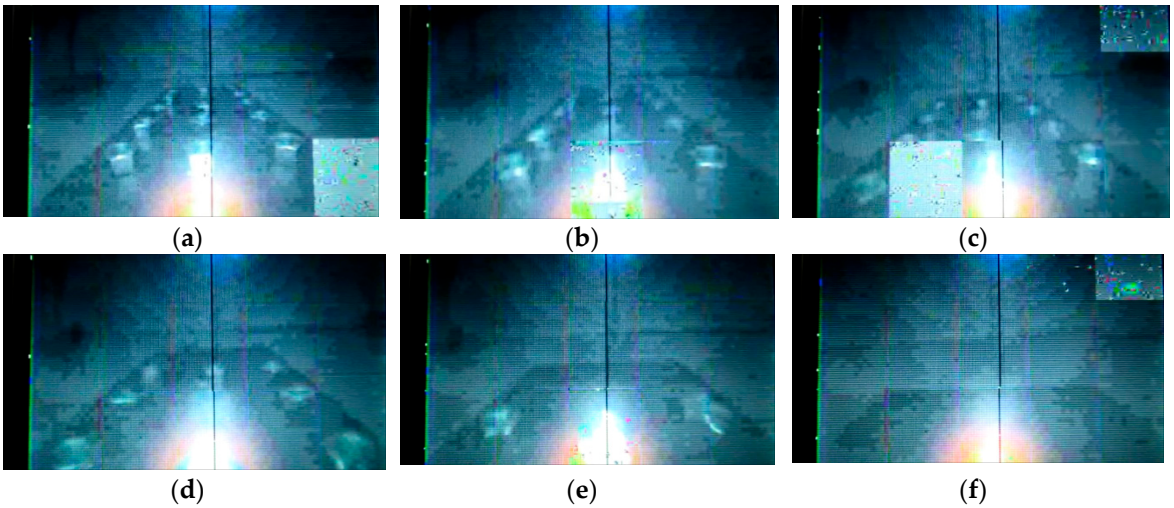

Figure 17. Images of camera attached to the front of BIREM with the control. (**a**) 0 s; (**b**) 2 s; (**c**) 4 s; (**d**) 6 s; (**e**) 8 s; (**f**) 10 s.

5. Conclusions

The aim of this study was to develop a robot for bridge inspection by creating a right and left two-wheel-drive robot called BIREM 3rd that runs through a right-angle path as well as a splicing part. The following results were obtained with respect to BIREM 3rd.

(1) The results confirmed that it was possible to run the robot on the inner right-angle path, where the robot is expected to run to inspect the damaged parts in the box girder. However, in contrast to the ordinary steel plates used in the laboratory, the magnetic force decreased from 25% to 40% for the steel members for bridges, and thus, it was necessary to replace all magnets in the robot with stronger magnets for actual field applications.

(2) The wheel track of BIREM 3rd is small (74 mm), and thus, the robot could run through the splicing part with bolts located at an interval of 75 mm by keeping the wheel from riding on the bolt or the nut on the splicing parts. However, rotatable-caster-type rear wheels are indispensable.

(3) It is very difficult for an operator to manually maneuver the robot to avoid bolts on the splicing part. However, the appropriate attachment of a camera and an LED on the robot enabled autonomous control, and thus, it was easy to maneuver the robot such that it could run through the splicing part.

Acknowledgments: The authors would like to express their gratitude to Kenichi Sugii and Tetsuya Unotsu, Hanshin Expressway Engineering Co. Ltd. (Osaka, Japan), for the research funds and for providing the experimental environments.

Author Contributions: Naoto Imajo and Satoshi Ito manufactured the BIREM 3rd and performed running experiments; Satoshi Ito performed the experiment for the autonomous control of the robot; Yogo Takada came up with the idea for the mechanism and visual control of BIREM 3rd and wrote the paper.

Conflicts of Interest: The authors declare no conflict of interest.

References

1. Watanabe, E.; Furuta, H.; Yamaguchi, T.; Kano, M. On longevity and monitoring technologies of bridges: A survey study by the Japanese Society of Steel Construction. *Struct. Infrastruct. Eng.* **2014**, *10*, 471–491. [CrossRef]
2. White Paper on Land, Infrastructure, Transport and Tourism in Japan, 2015. Available online: http://www.mlit.go.jp/en/statistics/white-paper-mlit-2015.html (accessed on 20 July 2017).
3. Nonami, K. Drone Technology, Cutting-Edge Drone Business, and Future Prospects. *J. Rob. Mechatronics* **2016**, *28*, 262–272. [CrossRef]

4. Higashi, Y.; Akahori, S.; Masuda, A.; Takeuchi, K. Verification of an EPM system for an Aerial Inspection Robot and Close-up Image Shooting. *Adv. Exp. Mech.* **2016**, *1*, 179–184.
5. Tokura, Y.; Toba, K.; Takada, Y. Practical Applications of HORNET to Inspect Walls of Structures. *J. Rob. Mechatronics* **2016**, *28*, 320–327. [CrossRef]
6. Mazumdar, A.; Asada, H.H. An Underactuated, Magnetic-Foot Robot for Steel Bridge Inspection. *J. Mech. Rob.* **2010**. [CrossRef]
7. iXs Research Corporation, SAUT ROBOT, Product introduction (in Japanese). Available online: http://www.ixs.co.jp/products/robot/saut-robot-j.html (accessed on 20 July 2017).
8. Zhu, D.; Guo, J.; Cho, C.; Wang, Y.; Lee, K.M. Wireless mobile sensor network for the system identification of a space frame bridge. *IEEE ASME Trans. Mechatron* **2012**, *17*, 499–507. [CrossRef]
9. Wang, R.; Kawamura, Y. An automated Sensing System for steel bridge inspection using GMR sensor array and magnetic wheels of climbing robot. *J. Sensors* **2016**. [CrossRef]
10. Takada, Y.; Kirimoto, K.; Tajiri, T.; Kawai, T. Development of a bridge inspection robot working in three-dimensional. *Trans. Jpn. Soc. Mech. Eng.* **2013**, *79*, 3135–3146. [CrossRef]
11. Imajo, N.; Takada, Y.; Kashinoki, M. Development and evaluation of compact robot imitating a hermit crab for inspecting the outer surface of pipes. *J. Rob.* **2015**. [CrossRef] [PubMed]
12. Chapter 7: Connections. In *Japan Road Association*; Maruzen Co. Ltd.: Tokyo, Japan, 2012; pp. 127–152. Available online: http://www.road.or.jp/books/pdf/07-002.pdf (assessed on 20 July 2017).